

pubs.acs.org/JACS Article

# Nanographene-Fused Expanded Carbaporphyrin Tweezers

Haodan He, Yu Jin Lee, Zhaohui Zong, Ningchao Liu, Vincent M. Lynch, Jinseok Kim, Juwon Oh,\* Dongho Kim,\* Jonathan L. Sessler,\* and Xian-Sheng Ke\*



Cite This: J. Am. Chem. Soc. 2024, 146, 543-551



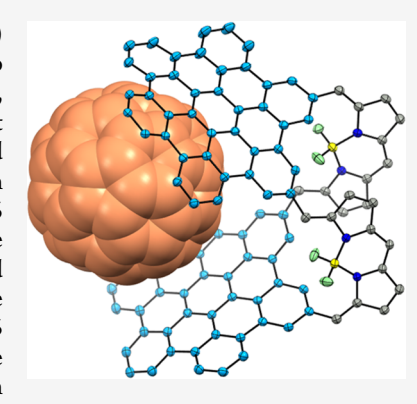
**ACCESS** I

Metrics & More

Article Recommendations

Supporting Information

**ABSTRACT:** A nanographene-fused expanded carbaporphyrin (5) and its BF<sub>2</sub> complex (6) were synthesized. Single-crystal X-ray structures revealed that 5 and 6 are connected by two hexa-peri-hexabenzocoronene (HBC) units and two dipyrromethene or BODIPY units, respectively. As prepared, 5 and 6 both show nonaromatic character with figure-of-eight carbaoctaphyrin (1.1.1.0.1.1.1.0) cores and adopt tweezers-like conformations characterized by a partially confined space between the two constituent HBC units. The distance between the HBC centers is >10 Å, while the dihedral angles between the two HBC planes are 30.5 and 35.2° for 5 and 6, respectively. The interactions between 5 and 6 and fullerene  $C_{60}$  were studied both in organic media and in the solid state. Proton NMR spectral titrations of 5 and 6 with  $C_{60}$  revealed a 1:1 binding mode for both macrocycles. In toluene- $d_8$ , the corresponding binding constants were determined to be 1141  $\pm$  17 and 994  $\pm$  10  $M^{-1}$  for 5 and 6, respectively. Single-crystal X-ray diffraction structural analyses confirmed the formation of 1:1 fullerene inclusion complexes in the solid state. The  $C_{60}$  guests in both



complexes are found within triangular pockets composed of two HBC units from the tweezers-like receptor most closely associated with the bound fullerene, as well as an HBC unit from an adjacent host. Femtosecond transient absorption measurements revealed subpicosecond ultrafast charge separation between 5 (and 6) and  $C_{60}$  in the complexes. To the best of our knowledge, the present report provides the first example wherein a nanographene building block is incorporated into the core of a porphyrinic framework.

## INTRODUCTION

Carbaporphyrins represent porphyrin analogues where one or more nitrogen donor atoms in the core are replaced by a carbon atom. They have attracted interest for their  $\pi$ conjugation pathways that differ from those of traditional tetrapyrrolic porphyrins as well as their own unique metal coordination chemistry. To date, polycyclic aromatic hydrocarbons (PAHs), such as naphthalene, 2-6 anthracene, 7-9 phenanthrene, 10-14 triphenylene, 15 and pyrene, 16-18 have been used to create carbaporphyrins. Recently, we reported that dibenzo [g,p] chrysene could serve as a building block to prepare a bis-dicarbacorrole, a highly twisted three-dimensional (3-D) cage structure, and a pyrene-containing belt-like system.  $^{19-22}$  However, to the best of our knowledge, large  $\pi$ extended PAHs, such as nanographenes, have yet to be introduced into carbaporphyrin frameworks. Were they available, such systems could advance our understanding of nanographene chemistry while providing potentially interesting new supramolecular receptors. The present study was undertaken in an effort to explore this promise.

Nanographenes are polyaromatic hydrocarbons that have attracted increasing synthetic attention due to their intriguing structures and potential utility in nanoelectronics, optoelectronics, and spintronics. <sup>23–27</sup> Compared to top-down preparative methods, such as the "cutting" of graphene and carbon nanotubes, bottom-up synthetic approaches can control more accurately the size, edge structure, and location of the

functionalities present in the nanographene.<sup>28</sup> Although known for decades, 29,30 it was only with the development of an efficient synthesis of hexa-peri-hexabenzocoronene (known as HBC) by Müllen and co-workers<sup>31</sup> that HBC-based nanographenes became readily amenable to synthesis. 32-34 Early on, in an effort to assess electronic communication between the HBC and porphyrin unit, Jux and co-workers synthesized the first directly linked HBC-porphyrin conjugate.<sup>35</sup> Subsequently, they reported several systems bearing multiple HBC or porphyrin units. 36-39 Guldi and co-workers further studied the interactions between HBC-porphyrin conjugates and fullerenes in both noncovalently linked supramolecular complexes and covalent-linked HBC-porphyrin-fullerene conjugates. 40-42 Currently, several other nano-graphene-porphyrin conjugates are known; 43-45 however, to our knowledge, introducing a nanographene unit into the core of a porphyrinic framework remains an unmet synthetic challenge.

In this work, two dipyrromethene units were used to connect two HBC units and form what we believe is the first

Received: September 14, 2023 Revised: December 13, 2023 Accepted: December 14, 2023 Published: December 26, 2023





Scheme 1. Synthesis of Carbaporphyrin Tweezers 5 and Its Bis-BF<sub>2</sub> Complex 6<sup>a</sup>

"Conditions: (i) 1,2-Bis(4-(tert-butyl)phenyl)ethyne in Ph<sub>2</sub>O, 260 °C, 5 h, 90%; (ii) DDQ and TfOH in CH<sub>2</sub>Cl<sub>2</sub>, 0 °C, 0.5 h, then RT, 5 h, 87%; (iii) n-BuLi in THF, – 78 °C, 1 h, then mesitaldehyde, – 78 °C, 1 h, 65%; (iv) dipyrromethane and BF<sub>3</sub>·OEt<sub>2</sub> in dry CH<sub>2</sub>Cl<sub>2</sub>, RT, 2 h, then DDQ, RT, 0.5 h, 7%; (v) DIPEA in toluene, 25 °C, 15 min, then BF<sub>3</sub>·OEt<sub>2</sub>, 80 °C, 24 h, 54%. Mes, t-Bu, and C<sub>6</sub>F<sub>5</sub> denote mesityl, tert-butyl, and pentafluorophenyl groups, respectively.

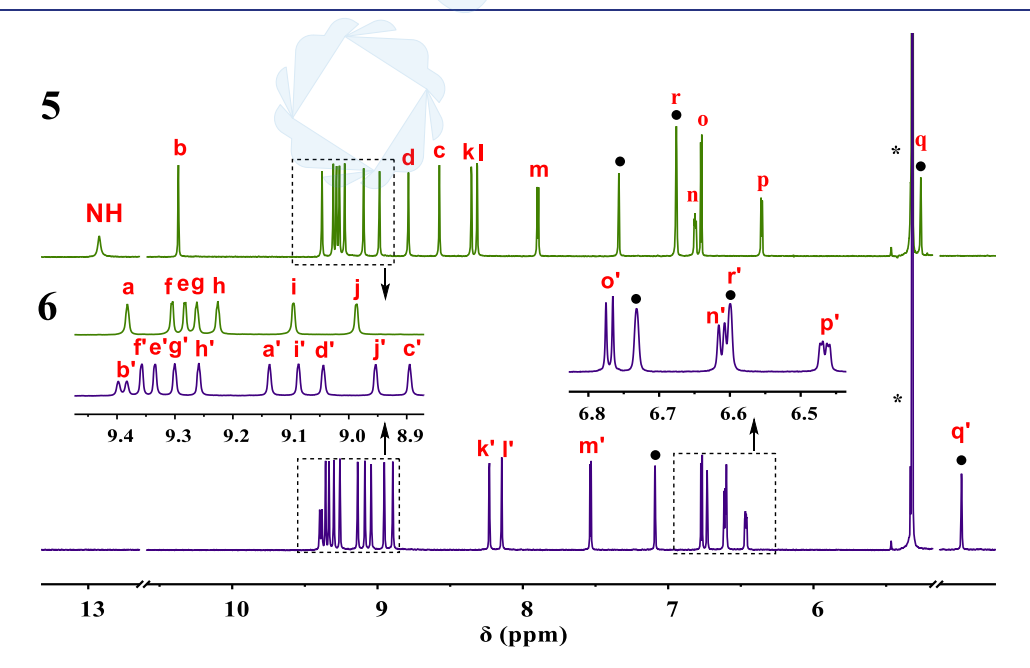


Figure 1. Partial  $^1$ H NMR spectra of 5 and 6 recorded in  $CD_2Cl_2$ . Dots indicate signals from the *meso*-mesityl groups, and asterisks indicate residual solvent peaks. The labeling refers to the features for only one set of proton signals due to symmetry.

HBC-fused carbaporphyrin (5). In contrast to earlier reported linked, as opposed to fused, nanographene-porphyrin systems, 5 adopts a figure-of-eight carbaoctaphyrin (1.1.1.0.1.1.1.0) core. 12 This twisting leads to a tweezers-like structure with a partially confined space that differs from a previously reported diphenanthrioctaphyrin<sup>12</sup> that also adopts a figure-of-eight conformation. Treating 5 with BF<sub>3</sub>·OEt<sub>2</sub> provides the corresponding BF<sub>2</sub>-chelated dipyrromethene complex 6 (i.e., a BODIPY-like analogue), which retains its tweezers-like conformation. Both 5 and 6 act as effective receptors for fullerene C<sub>60</sub>. A 1:1 binding stoichiometry dominates in toluene- $d_8$  solution with the corresponding binding constants being measured as  $1141 \pm 17$  and  $994 \pm 10$  M<sup>-1</sup> for 5 and 6, respectively. We further revealed subpicosecond ultrafast charge separation in the complexes  $5^{\circ}C_{60}$  and  $6^{\circ}C_{60}$ . In contrast to the many extensively studied 46-54 and in certain instances highly effective receptors based on curved building blocks, 55-57 our system is noteworthy for containing relatively planar HBC subunits. It also stands, to our knowledge, as the first expanded carbaporphyrin receptor-fullerene guest complex to be fully characterized both in organic media and in the solid state.

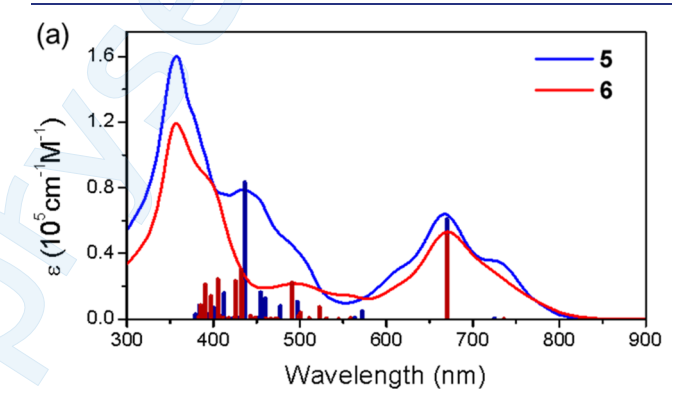
#### ■ RESULTS AND DISCUSSION

The synthesis of 5 and 6 is shown in Scheme 1. Intermediate 2 was prepared from the Diels-Alder reaction of known precursor 1 with 1,2-bis(4-(tert-butyl)phenyl) ethyne in Ph<sub>2</sub>O at reflux. Treatment with 2,3-dichloro-5,6-dicyano-pbenzoquinone (DDQ) in the presence of trifluoromethanesulfonic acid (TfOH) yielded the fused dibrominated intermediate 3. Reaction of 3 with mesitaldehyde in the presence of *n*-butyllithium yielded the bicarbinol 4. A BF<sub>3</sub>. OEt<sub>2</sub>-catalyzed [2 + 2] condensation between 4 and pentafluorophenyl-substituted dipyrromethane, followed by oxidation with DDQ, yielded 5 in 7% yield. Carbaporphyrin 5 was then treated with an excess of BF<sub>3</sub>·OEt<sub>2</sub> in the presence of N,N-diisopropylethylamine (DIPEA). After heating at reflux in toluene under N2, the BODIPY-like BF2-chelated dipyrromethene complex 6 was obtained in 54% yield. Both 5 and 6 were characterized by <sup>1</sup>H, <sup>19</sup>F, two-dimensional correlation spectroscopy (2D COSY), nuclear Överhauser effect (NOE), NMR and UV-vis-NIR spectroscopies, as well as high-resolution matrix-assisted laser desorption/ionization time-of-flight (HR-MALDI-TOF) mass spectrometry, and single-crystal X-ray diffraction analyses.

The <sup>1</sup>H NMR spectra of 5 and 6 were recorded in CD<sub>2</sub>Cl<sub>2</sub> (Figure 1). The resonances for 5 and 6 could be readily assigned from the corresponding 2D COSY and NOE spectra (Figures S36–S39 and S43–S46). In the case of 5, the pyrrolic  $\beta$ -CH protons were found to resonate at 7.90, 6.81, 6.78, and 6.35 ppm (labeled with H<sup>m</sup>, H<sup>n</sup>, H<sup>o</sup>, and H<sup>p</sup>, respectively). The signals at 9.38 and 10.37 ppm were assigned to the CH protons within the carbaporphyrin macrocycle (inner CHs, labeled with H<sup>a</sup> and H<sup>b</sup>). The other signals from the CH protons (H<sup>c</sup> to H<sup>1</sup>) on the HBC backbone could also be readily assigned, with chemical shifts ranging from 8.31 to 9.30 ppm. The NH signal is observed at 12.92 ppm, as confirmed by a D<sub>2</sub>O exchange experiment (Figure \$35). The average chemical shift difference between the pyrrolic NH and  $\beta$ -CHs proton signals  $(\Delta\delta)$  was found to be 5.96 ppm. The value is comparable to what was reported for a nonaromatic carbaporphyrin cage (5.98 ppm).<sup>21</sup> Thus, macrocycle 5 is best considered as nonaromatic. It should also be noted that there is one mesityl group located between two HBC units. This orientation leads to an upfield shifting of the corresponding proton signals. For instance, the  $H^q$  and  $H^s$  protons on the mesityl group (highlighted in purple) are found to resonate at 5.26 and 0.64 ppm, respectively (Figure S34).

In the bis-BF<sub>2</sub> complex **6**, the pyrrolic  $\beta$ -CH signals are assigned at 7.54, 6.61, 6.78, and 6.47 ppm (labeled with  $H^{m'}$ ,  $H^{n'}$ ,  $H^{n'}$ , and  $H^{p'}$ , respectively). The signals of the inner CHs ( $H^{a'}$  and  $H^{b'}$ ) appear at 9.14 and 9.39 ppm and are shifted upfield relative to  $H^a$  and  $H^b$  in the free base macrocycle **5**. The remainder of the CH proton signals ( $H^{c'}$  to  $H^{l'}$ ) on the HBC backbone appear between 8.15 and 9.36 ppm. In addition, the original NH signal disappears and two new sets of BODIPY-like peaks appear in the <sup>19</sup>F NMR spectrum (Figures S42 and S47). Compared to the free base **5**, the chemical shifts of the  $H^{q'}$  and  $H^{s'}$  protons of the mesityl group of the bis-BF<sub>2</sub> complex **6** are shifted upfield (to 4.39 and 0.09 ppm, respectively), reflecting what are presumably enhanced shielding effects.

The UV-vis-NIR absorption spectra of 5 and 6 were recorded in toluene and are shown in Figure 2a. In the case of



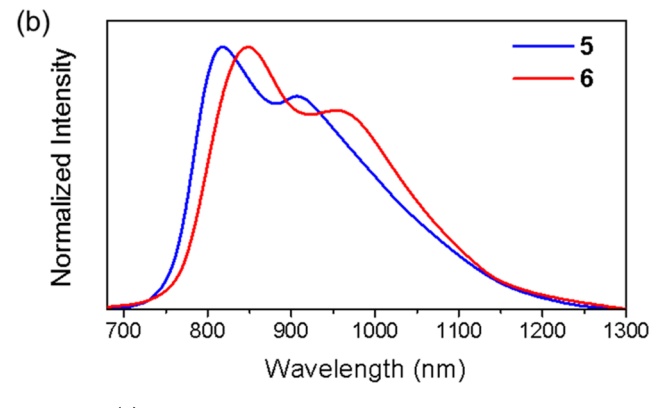


Figure 2. (a) UV-vis-NIR absorption spectra and corresponding calculated oscillator strengths and (b) fluorescence spectra of 5 and 6 recorded in toluene by using an excitation wavelength of 670 nm.

5, an intense absorption band at 356 nm with a shoulder at 434 nm is seen, along with a broad absorption feature centered at 668 nm and a shoulder at 725 nm. For the bis-BF<sub>2</sub> complex 6, an intense band at 357 nm is observed, along with a broad band centered at 672 nm and a very weak absorption at 495 nm. Compared to the free base 5, the molar extinction coefficient of 6 is slightly lower, and the shoulder features are less pronounced. Meanwhile, 5 and 6 show weak NIR fluorescence in the range of 700–1300 nm (Figure 2b). Along with their lowest absorption bands in the range of 600–

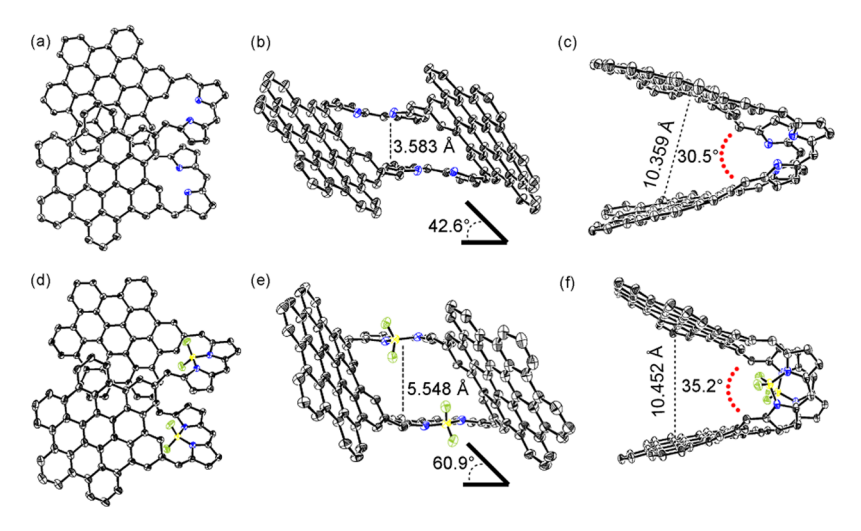


Figure 3. X-ray structures of 5 shown in (a) front, (b) side, and (c) top views; and 6 in (d) front, (e) side, and (f) top views. The thermal ellipsoids are scaled to the 50% probability level. Solvent molecules, hydrogen atoms, *meso*-aryl substituents, and *tert*-butyl groups are omitted for clarity.

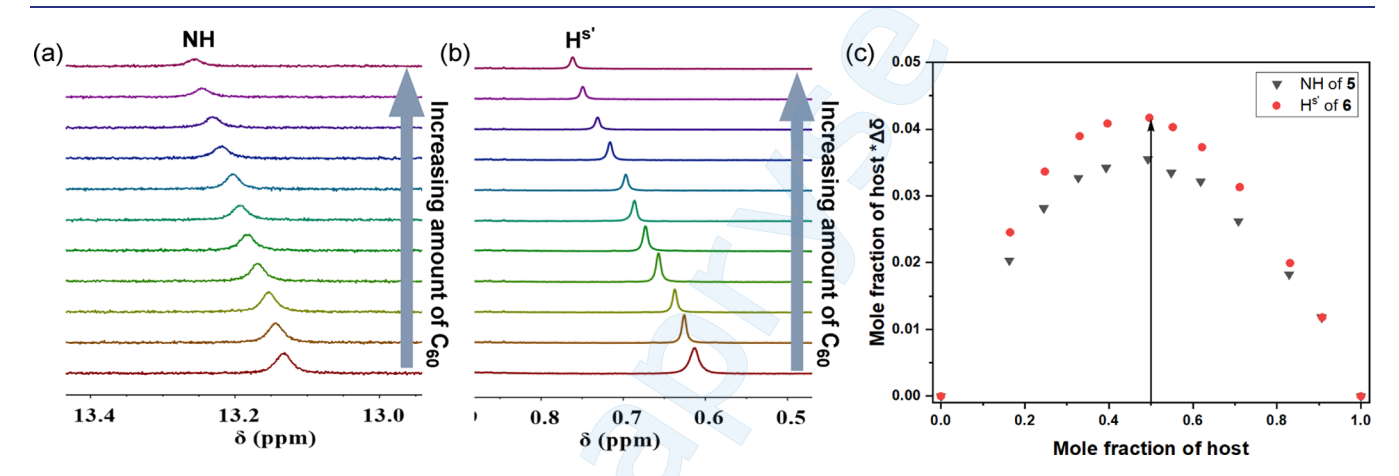


Figure 4. (a) Changes in the chemical shift of the inner NH proton resonance seen in a  $^{1}$ H NMR titration of 5 with  $C_{60}$  in toluene- $d_{8}$  where the starting concentration of the receptor was 0.95 mM; (b) changes in the chemical shift of the H $^{5\prime}$  proton resonance seen in a  $^{1}$ H NMR spectroscopic titration of 6 with  $C_{60}$  in tolene- $d_{8}$  where the starting concentration of the receptor was 1.0 mM; (c) Job plot constructed from the chemical shift changes seen during  $^{1}$ H NMR spectral titrations of 5 or 6 with  $C_{60}$  in toluene- $d_{8}$  using the same starting concentrations as in (a) and (b).

800 nm, these NIR fluorescence features of **5** and **6** are taken as evidence of effective  $\pi$ -conjugative interactions between the core (dipyrromethene and BODIPY) and the nanographene units. This coupling is also reflected in the results of the time-dependent density-functional theory (TD-DFT) calculations for **5** and **6**. Based on this latter analysis, their lowest absorption bands mainly arise from electronic transitions among highest occupied molecular orbital (HOMO) -1, HOMO, lowest unoccupied molecular orbital (LUMO), and LUMO + 1 molecular orbital (Tables S1 and S2). Notably in both **5** and **6**, the core electron densities spread well beyond the central dipyrromethene and BODIPY subunits to include both flanking nanographene units (Figure S4).

The electrochemical properties of 5 and 6 were investigated by cyclic voltammetry (CV) and differential pulse voltammetry (DPV) (Figure S1). The first oxidation and reduction potentials of 5 were found to be 0.17 and -1.54 V (vs Fc $^+$ /Fc), respectively, which leads to an electrochemical HOMO–LUMO gap of 1.71 eV. The corresponding electrochemical HOMO–LUMO gap was determined to be 1.78 eV in the case of 6 based on first oxidation and reduction potentials of 0.35 and -1.43 V (vs Fc $^+$ /Fc), respectively. These HOMO–

LUMO gaps reflect the UV-vis absorption spectra and match well the HOMO-LUMO energy gaps (1.974 and 2.050 eV for 5 and 6, respectively) estimated by density functional theory (DFT) at the B3LYP/6-31G(d,p) level (Figure S4 and Table S3).

Diffraction-grade single crystals of 5 were grown from acetonitrile/hexanes. The resulting structures confirmed the formation of the target macrocycle and its tweezers-like conformation (Figure 3). Compound 5 consists of two HBC units connected by two dipyrromethene units. The nonhydrogen atoms in the backbone appear to be sp<sup>2</sup> hybridized, which is as expected for a structure that is fully conjugated. The center-to-center distance between the two HBC units is 10.359 Å (centroids based on the 42 carbon atoms of the HBC backbone), whereas the dihedral angle between the two HBC planes (mean plane defined by all 42 carbon atoms of the HBC backbone) is 30.5°. The two dipyrromethene units are nearly parallel with a mean plane (defined by all 11 atoms of the dipyrromethene backbone) distance of 3.583 Å. The dihedral angles between the dipyrromethene and HBC planes show similar values of 41.0, 42.6, 42.7, and 44.1°, respectively; thus, the average angle can be calculated as 42.6° (Figure S26).

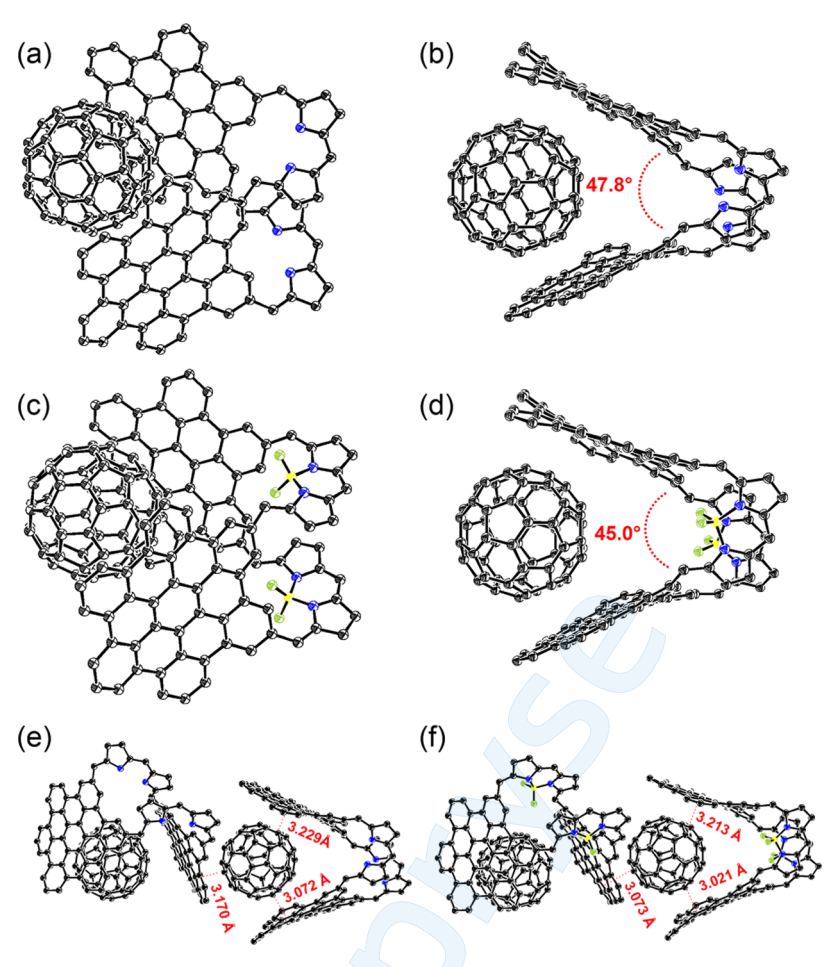


Figure 5. Single-crystal structures of  $5 \cdot C_{60}$  shown in (a) front and (b) top views and of  $6 \cdot C_{60}$  shown in (c) front and (d) top views; more extended views of (e) the interactions between  $C_{60}$  and 5 and (f) between  $C_{60}$  and 6. Thermal ellipsoids are scaled to the 50% probability level. Solvent molecules, hydrogen atoms, *meso*-aryl substituents, and *tert*-butyl groups are omitted for clarity.

Overall, the tweezers-like molecules pack in a zigzag pattern. The two HBC planes of the adjacent repeat units are parallel to each other, and the corresponding separation distances are about 3.548 and 3.589 Å (Figures S22 and S23). These values, which are less than the sum of the van der Waals radii, indicate that the  $\pi$ - $\pi$  interaction plays a key role in the packing. In addition, some nearest carbon—carbon distances between the methyls of the mesityl and *tert*-butyl substituents and adjacent HBC backbone are about 3.646–3.721 Å. The nearest fluorine atom on the pentafluorophenyl group was found at a distance of 3.166 Å from the corresponding HBC plane, leading us to suggest that CH- $\pi$  and F- $\pi$  interactions also contribute to the observed stacked arrangement (Figures S22 and S23).

Diffraction-grade single crystals of bis-BF<sub>2</sub> complex 6 were grown from toluene/methanol (Figure 3). The corresponding structure revealed that the dihedral angle between the two HBC planes had increased to 35.2° relative to 5 and that the average dihedral angle between the two BODIPY planes (mean plane defined by all 12 atoms except for the F atoms of the BODIPY backbone) and the two HBC planes increased to 60.9° (Figure S26). The distance between the two nearly parallel BODIPY units increased to 5.548 Å (Figure 3e). These structural changes are ascribed to increases in both steric hindrance and rigidity relative to 5. The packing diagram revealed that 6 also adopts a zigzag arrangement in the solid state; however, unlike 5, the two molecules within the individual repeat units are embedded within their respective

cavities (Figures S24 and S25). The distances from the *tert*-butyl methyl groups, mesityl methyl groups, and the fluorine atoms on the pentafluorophenyl substituents to the nearest HBC plane were found to vary from 3.119 to 3.721 Å. In contrast to 5, the distance between the two paralleled adjacent HBC planes in 6 is about 4.410 Å, a finding that rules out appreciable  $\pi-\pi$  interactions. Thus, the stacking seen in the case of 6 is thought to reflect CH $-\pi$  and F $-\pi$  interactions (Figures S24 and S25).

In order to test whether molecular tweezers 5 and 6 could act as supramolecular receptors, toluene-d<sub>8</sub> solutions were subjected to <sup>1</sup>H NMR spectroscopic titrations using C<sub>60</sub> as a putative substrate (Figures 4, S7, and S13). In the case of 5, a continuous variation plot was constructed using changes in the signal for the inner NH proton and one of the methyl protons from the mesityl (Mes) substituent (H<sup>s</sup>) in the shielded area. This Job plot and standard curve fitting allowed a 1:1 binding constant  $(K_a)$  of 1141  $\pm$  17 M<sup>-1</sup> to be derived (Figure S9). For 6, protons on the HBC backbone (Har) and a Mes methyl signal  $(H^{s\prime})$  proved to be the easiest to monitor; this allowed a 1:1  $K_a$  of 994  $\pm$  10 M<sup>-1</sup> to be derived (Figure S15). We speculate that the slightly lower affinity seen in the case of 6 reflects the increased rigidity of the framework, which in turn makes it more difficult for the  $C_{60}$  to be accommodated within the tweezers-like cavity.

Compared to a reported macrocyclic heptagon-containing nanographene, for which a  $K_a = 420 \pm 2 \text{ M}^{-1}$  was derived

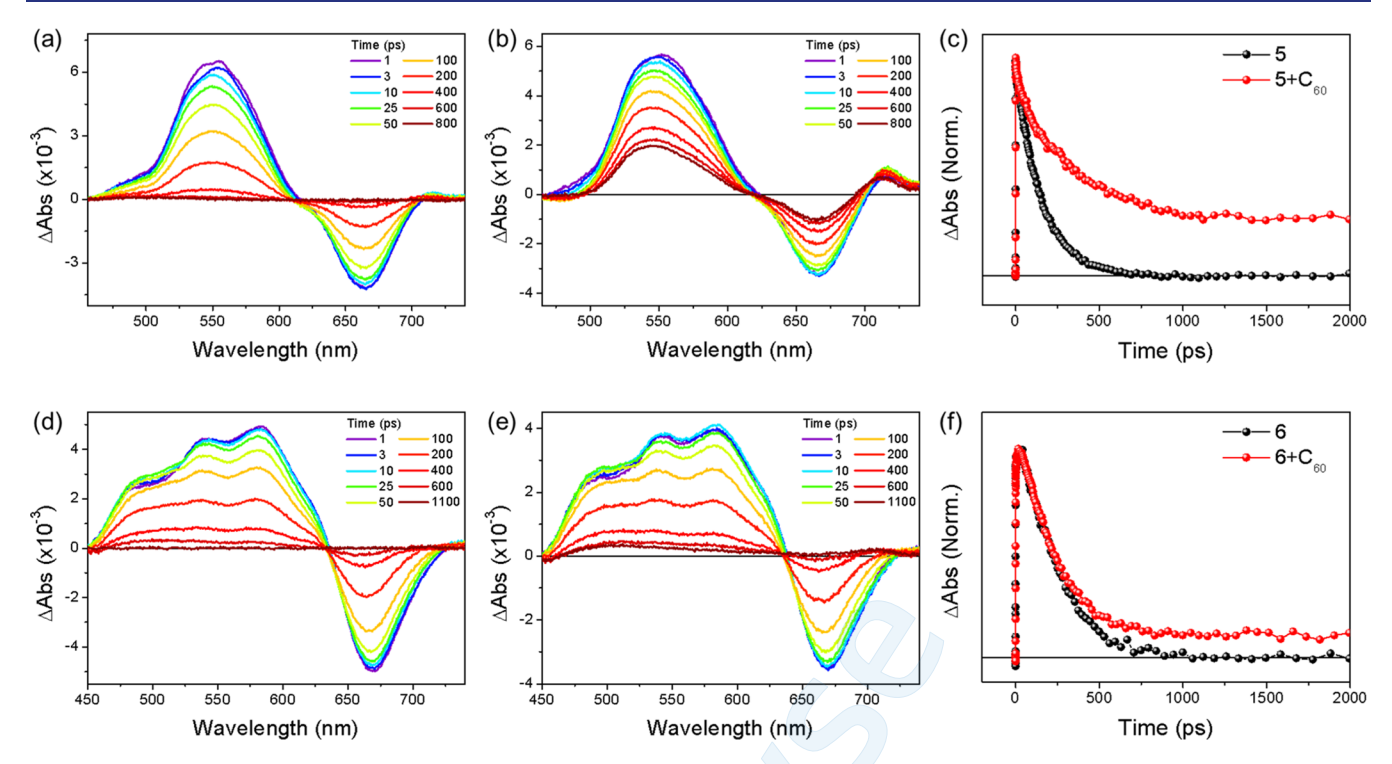


Figure 6. Transient absorption spectra of (a) 5, (b) 6, (d) 5 with excess  $C_{60}$  and (e) 6 with excess  $C_{60}$  in toluene with photoexcitation at 400 nm and (c, f) their decay profiles at 560 nm.

based on a  $^1\mathrm{H}$  NMR spectroscopic titration in  $o\text{-DCB-}d_4$ ,  $^{53}$  the affinities of 5 and 6 for C $_{60}$  are roughly 2-fold higher. Note: to allow comparisons to this prior system, receptor 5 was subjected to titration with C $_{60}$  in ODCB- $d_4$ . A  $K_a$  value of approximately 1300 M $^{-1}$  was obtained (Figures S10–S12). The  $K_a$  values for 5 and 6 are comparable to that of a doubly curved nanographene, for which a  $K_a$  of 1170  $\pm$  2 M $^{-1}$  was reported based on  $^1\mathrm{H}$  NMR spectroscopic titrations carried out in toluene- $d_8$ .  $^{52}$  A  $^1\mathrm{H}$  NMR spectroscopic titration between C $_{60}$  and hexa-tert-butylhexabenzocoronene (a known HBC monomer, synthesized for comparison; Figure S16) revealed only modest changes that failed to yield reliable binding constants when fitted to a 1:1, 1:2, or 2:1 binding model (Figures S17–S21). On this basis, we conclude that the tweezers-like conformation inherent in 5 and 6 serves to increase the ability of the planar HBC subunits to interact with the curved fullerene surface of C $_{60}$ .

Single crystals of the 1:1 complex of 5 and  $C_{60}$  (5· $C_{60}$ ) were grown by allowing n-heptane to diffuse into a toluene solution containing the host (5) and guest (C<sub>60</sub>) in a 1:1 molar ratio (Figure 5). As expected, the  $C_{60}$  molecule was found to reside between the two HBC planes. Compared to the fullerene-free host 5, the HBC backbone in  $5 \cdot C_{60}$  is slightly distorted. The angle between the two HBC planes of 5°C<sub>60</sub> is seen to increase to 47.8°, while the average angle between the HBC and the dipyrromethene planes increases to 53.4° (the individual dihedral angles are 49.1, 50.3, 57.1, and 57.3°; Figure S26). The distances between the nearest carbon of the  $C_{60}$  molecule and the two HBC planes are 3.072 and 3.229 Å, respectively; this is as would be expected for a complex wherein  $\pi - \pi$ interactions between the C<sub>60</sub> and the two HBC arms play a stabilizing role. Several of the phenyl CH protons and those of the mesityl methyl groups, as well as some tert-butyl groups on the edge of the HBC units, appear to interact with the  $C_{60}$  via weak CH $-\pi$  bonds as evidenced by carbon–carbon distances

that vary from 3.438 to 3.914 Å (Figure S28). A third HBC unit on an adjacent host molecule was found to interact with the  $C_{60}$  guest (Figure 5e) as inferred from the 3.170 Å separation between the fullerene and the closest carbon on this adjacent HBC unit.

Single crystals of the 1:1 complex of 6 and  $C_{60}$  were grown by allowing n-heptane to diffuse into a toluene solution containing the host (6) and guest ( $C_{60}$ ) in a 1:1 molar ratio (Figure 5). As true for  $\mathbf{5 \cdot C_{60}}$ , the tweezers-like structure in  $\mathbf{6 \cdot C_{60}}$  is wider than in the free host 6, as reflected in a dihedral angle between the two HBC planes in  $\mathbf{6 \cdot C_{60}}$  that increase to  $45.0^{\circ}$  and average angles between the dipyrromethene and HBC planes that are now  $64.9^{\circ}$  (Figure S26). The fullerene molecule in  $\mathbf{6 \cdot C_{60}}$  is found within a triangular pocket made up of two HBC units from one host and an HBC unit from an adjacent host. The nearest carbon on the  $C_{60}$  guest is separated from these three HBC planes by distances of 3.021, 3.213, and 3.073 Å, respectively, leading to the inference that  $\pi - \pi$  donor—acceptor interactions also contribute to the complexation of  $C_{60}$  in the case of BODIPY complex 6.

We further examined the complexation of **5** and **6** with  $C_{60}$  by means of UV-vis-NIR absorption measurements (Figure S2). Although the spectral changes for **5** and **6** were modest upon titration with  $C_{60}$ , clear isosbestic points were seen, as would be expected for the clean formation of  $5 \cdot C_{60}$  and  $6 \cdot C_{60}$ . Upon complex formation, the lowest absorption bands of **5** and **6** are attenuated. Similar spectral changes were observed in a previous study involving the complexation of  $C_{60}$  by an expanded porphyrin. <sup>58</sup>

To unveil the excited-state dynamics of complexes  $5 \cdot C_{60}$  and  $6 \cdot C_{60}$ , we carried out transient absorption (TA) measurements (Figure 6). Both 5 and 6 show decay in their TA spectra within 1 ns, reflecting excited-state lifetimes of 160 and 220 ps for 5 and 6, respectively. An increase in the TA spectral decay with a long residual TA signal was seen upon treatment of 5 and 6

with an excess of  $C_{60}$ . Moreover, compared with the TA spectra of **5**, an additional excited-state absorption band is observed at 730 nm in the TA spectra of **5** in the presence of excess  $C_{60}$ . These TA features are consistent with the generation of long-lived charge-separated species following photoexcitation of  $\mathbf{5} \cdot \mathbf{C}_{60}$  and  $\mathbf{6} \cdot \mathbf{C}_{60}$ . DFT calculations revealed binding energies of -10.3 and -10.5 kJ/mol in the case of  $\mathbf{5} \cdot \mathbf{C}_{60}$  and  $\mathbf{6} \cdot \mathbf{C}_{60}$ , respectively (Figure S5). The corresponding HOMO and LUMO analyses provide a clear rationale for the photoinduced electron transfer from **5** (and **6**) to  $\mathbf{C}_{60}$  (Figure S6).

It is noteworthy that the TA spectra of 5 with excess  $C_{60}$ contains initially an additional excited-state absorption band at 730 nm as compared to the spectra recorded for 5 alone (Figure S3a,b). This indicates that an ultrafast electron transfer process in 5.C60 occurs within our TA Instruments time resolution (~200 fs). On the other hand, no apparent TA spectral signals ascribable directly to the formation of 6.C60 are seen, the TA decay profiles of 6 with an excess of C<sub>60</sub> show a rise component within the initial delay time (~10 ps) with a time constant of 800 fs (Figure S3c,d). This feature is not observed in the TA spectrum of 6 and is thus ascribed to a subpicosecond ultrafast charge separation process within 6.C60. The electron transfer event seen in the fullerene complexes 5. C<sub>60</sub> and 6·C<sub>60</sub> are thought to reflect a delocalization of electron density from the core (dipyrromethene and BODIPY) to the peripheral nanographene units in 5 and 6 as well as effective electron transfer to the bound C<sub>60</sub> through nanographene-C<sub>60</sub>  $\pi$ - $\pi$  interactions.

## CONCLUSIONS

In summary, we synthesized and characterized a new nanographene-fused expanded carbaporphyrin. This hybrid system contains two covalently linked nanographene units with large  $\pi$ -surfaces. The as-prepared free base form (5) can be easily functionalized by treating with BF<sub>3</sub>·OEt<sub>2</sub> to form a BODIPY-type complex, 6. Both 5 and 6 adopt tweezers-like conformation and bind C<sub>60</sub> well, in contrast to what is seen for a planar HBC monomer prepared as a control system. The present work provides a nexus between expanded porphyrin and nanographene chemistry and sets the stage for the synthesis and study of new molecular systems that display novel electronic features and act as receptors for relatively large substrates.

# ASSOCIATED CONTENT

#### Supporting Information

The Supporting Information is available free of charge at https://pubs.acs.org/doi/10.1021/jacs.3c10122.

Experimental details and characterization data (PDF)

## **Accession Codes**

CCDC 2286185, 2286187, and 2286189—2286190 contain the supplementary crystallographic data for this paper. These data can be obtained free of charge via www.ccdc.cam.ac.uk/data\_request/cif, or by emailing data\_request@ccdc.cam.ac.uk, or by contacting The Cambridge Crystallographic Data Centre, 12 Union Road, Cambridge CB2 1EZ, UK; fax: +44 1223 336033.

#### AUTHOR INFORMATION

## **Corresponding Authors**

Juwon Oh − Department of Chemistry, Soonchunhyang University, Asan 31538, Korea; orcid.org/0000-0003-0865-7595; Email: juwoh933@sch.ac.kr

Dongho Kim — Department of Chemistry, Yonsei University, Seoul 03722, Korea; ⊙ orcid.org/0000-0001-8668-2644; Email: dongho@yonsei.ac.kr

Jonathan L. Sessler — Department of Chemistry, The University of Texas at Austin, Austin, Texas 78712-1224, United States; orcid.org/0000-0002-9576-1325; Email: sessler@cm.utexas.edu

Xian-Sheng Ke — College of Chemistry, Beijing Normal University, Beijing 100875, China; ⊚ orcid.org/0000-0002-0562-1039; Email: kexiansheng@bnu.edu.cn

#### Authors

Haodan He – College of Chemistry, Beijing Normal University, Beijing 100875, China

Yu Jin Lee – Department of Chemistry, Yonsei University, Seoul 03722, Korea

Zhaohui Zong - College of Chemistry, Beijing Normal University, Beijing 100875, China

Ningchao Liu – College of Chemistry, Beijing Normal University, Beijing 100875, China

Vincent M. Lynch — Department of Chemistry, The University of Texas at Austin, Austin, Texas 78712-1224, United States Jinseok Kim — Department of Chemistry, Yonsei University, Seoul 03722, Korea

Complete contact information is available at: https://pubs.acs.org/10.1021/jacs.3c10122

# **Author Contributions**

H.H. and Y.J.L. contributed equally to this paper.

#### Notes

The authors declare no competing financial interest.

## ACKNOWLEDGMENTS

The work at Beijing Normal University (BNU) was supported by National Science Foundation of China (grant no. 22275020 to X.-S.K.) and startup funding (grant no. 312232114 to X.-S.K.). The work at Yonsei University was supported by the National Research Foundation of Korea (NRF) funded by the Korea Government (MSIT) (grant nos. 2020R1A5A1019141 and 2021R1A6A1A03039503). The quantum mechanical calculations were performed using the supercomputing resources of the Korea Institute of Science and Technology Information. The work in Austin was supported by the Robert A. Welch Foundation (F-0018 to J.L.S.) and by the National Science Foundation (CHE-2304731) subsequent to Nov. 1, 2023.

## REFERENCES

- (1) Lash, T. D. Carbaporphyrinoid systems. *Chem. Rev.* **2017**, *117* (4), 2313–2446.
- (2) Lash, T. D.; Young, A. M.; Rasmussen, J. M.; Ferrence, G. M. Naphthiporphyrins. *J. Org. Chem.* **2011**, *76* (14), 5636–5651.
- (3) Szyszko, B.; Latos-Grażyński, L. Conformational flexibility of 1,4-naphthiporphyrin promotes a palladium-mediated contraction of naphthalene to isoindene. *Organometallics* **2011**, *30* (16), 4354–4363.
- (4) Szyszko, B.; Pacholska-Dudziak, E.; Latos-Grazynski, L. Incorporation of the 1,5-naphthalene subunit into heteroporphyrin

- structure: Toward helical aceneporphyrinoids. *J. Org. Chem.* **2013**, 78 (10), 5090–5095.
- (5) Hong, J. H.; Aslam, A. S.; Ishida, M.; Mori, S.; Furuta, H.; Cho, D. G. 2-(naphthalen-1-yl)thiophene as a new motif for porphyrinoids: Meso-fused carbaporphyrin. *J. Am. Chem. Soc.* **2016**, *138* (15), 4992–4995.
- (6) Hong, J. H.; Aslam, A. S.; Cho, B.; Ko, M. S.; Kim, Y.; Heo, J.; Cho, D. G. Carbaporphyrin dimers that bear a rigid naphthalene motif as an internal strap. *Org. Lett.* **2021**, *23* (5), 1846–1850.
- (7) Szyszko, B.; Latos-Grazynski, L.; Szterenberg, L. Toward aceneporphyrinoids: Synthesis and transformations of palladium(II) meso-anthriporphyrin. Chem. Commun. 2012, 48 (41), 5004–5006.
- (8) Sung, Y. M.; Szyszko, B.; Mysliborski, R.; Stepien, M.; Oh, J.; Son, M.; Latos-Grazynski, L.; Kim, D. The effect of  $\pi$ -conjugation in the macrocyclic ring on the photophysical properties of a series of thiaaceneporphyrinoids. *Chem. Commun.* **2014**, *50* (61), 8367–8369.
- (9) Aslam, A. S.; Hong, J. H.; Shin, J. H.; Cho, D. G. Synthesis of a phlorin from a meso-fused anthriporphyrin by a Diels-Alder strategy. *Angew. Chem., Int. Ed.* **2017**, *56* (51), 16247–16251.
- (10) Szyszko, B.; Bialonska, A.; Szterenberg, L.; Latos-Grazynski, L. Phenanthriporphyrin: An antiaromatic aceneporphyrinoid as a ligand for a hypervalent organophosphorus(V) moiety. *Angew. Chem., Int. Ed.* **2015**, *54* (16), 4932–4936.
- (11) Szyszko, B.; Malecki, M.; Berlicka, A.; Bialek, M. J.; Bialonska, A.; Kupietz, K.; Pacholska-Dudziak, E.; Latos-Grazynski, L. Incorporation of a phenanthrene subunit into a sapphyrin framework: Synthesis of expanded aceneporphyrinoids. *Chem. Eur. J.* **2016**, 22 (22), 7602–7608.
- (12) Szyszko, B.; Chmielewski, P. J.; Przewoźnik, M.; Białek, M. J.; Kupietz, K.; Białońska, A.; Latos-Grażyński, L. Diphenanthrioctaphyrin (1.1.1.0.1.1.1.0): Conformational switching controls the stereochemical dynamics of the topologically chiral system. *J. Am. Chem. Soc.* 2019, 141 (14), 6060–6072.
- (13) Szyszko, B.; Przewoźnik, M.; Białek, M. J.; Białońska, A.; Chmielewski, P. J.; Cichos, J.; Latos-Grażyński, L. Helicenophyrins: Expanded carbaporphyrins incorporating aza[5]helicene and heptacyclic S-Shaped aza[5]helicene motifs. *Angew. Chem., Int. Ed.* **2018**, 57 (15), 4030–4034.
- (14) Kupietz, K.; Białek, M. J.; Białońska, A.; Szyszko, B.; Latos-Grażyński, L. Aromaticity control via modifications of a macrocyclic frame: 5,6-dimethoxyphenanthriporphyrin and 5,6-dioxophenanthriporphyrin. *Org. Chem. Front.* **2018**, *5* (21), 3068–3076.
- (15) Gopee, H.; Kong, X.; He, Z.; Chambrier, I.; Hughes, D. L.; Tizzard, G. J.; Coles, S. J.; Cammidge, A. N. Expanded porphyrin-like structures based on twinned triphenylenes. *J. Org. Chem.* **2013**, 78 (18), 9505–9511.
- (16) Gao, R.; AbuSalim, D. I.; Lash, T. D. Pyreniporphyrins: Porphyrin analogues that incorporate a polycyclic aromatic hydrocarbon subunit within the macrocyclic framework. *J. Org. Chem.* **2017**, 82 (13), 6680–6688.
- (17) Liang, K.; Chen, H.; Wang, X.; Lu, T.; Duan, Z.; Sessler, J. L.; Lei, C. Di-2,7-pyrenidecaphyrin(1.1.0.0.0.1.1.0.0.0) and its bisorganopalladium complexes: Synthesis and chiroptical properties. *Angew. Chem.* **2023**, *62* (3), No. e202212770.
- (18) Liu, L.; Zhang, F.; Xu, L.; Zhou, M.; Yin, B.; Tanaka, T.; Osuka, A.; Song, J. *m*-Benziporphyrin(1.1.0.0)s as a rare example of ring-contracted carbaporphyrins with metal-coordination ability: Distorted coordination structures and small HOMO-LUMO gaps. *Chem. Eur. J.* **2023**, *29* (14), No. e202203517.
- (19) Ke, X.-S.; Hong, Y.; Tu, P.; He, Q.; Lynch, V. M.; Kim, D.; Sessler, J. L. Hetero Cu(III)—Pd(II) complex of a dibenzo[g,p]-chrysene-fused bis-dicarbacorrole with stable organic radical character. *J. Am. Chem. Soc.* **2017**, 139 (42), 15232—15238.
- (20) Ke, X.-S.; Hong, Y.; Lynch, V. M.; Kim, D.; Sessler, J. L. Metalstabilized quinoidal dibenzo[ *g, p*]chrysene-fused bis-dicarbacorrole system. *J. Am. Chem. Soc.* **2018**, *140* (24), 7579–7586.
- (21) Ke, X.-S.; Kim, T.; He, Q.; Lynch, V. M.; Kim, D.; Sessler, J. L. Three-dimensional fully conjugated carbaporphyrin cage. *J. Am. Chem. Soc.* **2018**, *140* (48), 16455–16459.

- (22) Wang, Y.; Ke, X.-S.; Lee, S.; Kang, S.; Lynch, V. M.; Kim, D.; Sessler, J. L. Pyrene-bridged expanded carbaporphyrin nanobelts. *J. Am. Chem. Soc.* **2022**, *144* (21), 9212–9216.
- (23) Li, X.; Wang, X.; Zhang, L.; Lee, S.; Dai, H. Chemically derived, ultrasmooth graphene nanoribbon semiconductors. *Science* **2008**, *319* (5867), 1229–1232.
- (24) Ponomarenko, L. A.; Schedin, F.; Katsnelson, M. I.; Yang, R.; Hill, E. W.; Novoselov, K. S.; Geim, A. K. Chaotic dirac billiard in graphene quantum dots. *Science* **2008**, 320 (5874), 356–358.
- (25) Narita, A.; Wang, X. Y.; Feng, X.; Müllen, K. New advances in nanographene chemistry. Chem. Soc. Rev. 2015, 44 (18), 6616–6643.
- (26) Segawa, Y.; Ito, H.; Itami, K. Structurally uniform and atomically precise carbon nanostructures. *Nat. Rev. Mater.* **2016**, *1* (1), No. 15002.
- (27) Koga, Y.; Kaneda, T.; Saito, Y.; Murakami, K.; Itami, K. Synthesis of partially and fully fused polyaromatics by annulative chlorophenylene dimerization. *Science* **2018**, *359* (6374), 435–439.
- (28) Wang, X.-Y.; Narita, A.; Müllen, K. Precision synthesis versus bulk-scale fabrication of graphenes. *Nat. Rev. Chem.* **2018**, 2 (1), No. 0100.
- (29) Clar, E.; Ironside, C. T. Hexabenzocoronene. Proc. Chem. Soc. 1958, 150–151.
- (30) Hendel, W.; Khan, Z. H.; Schmidt, W. Hexa-peri-benzocoronene, a candidate for the origin of the diffuse interstellar visible absorption bands? *Tetrahedron* 1986, 42 (4), 1127–1134.
- (31) Stabel, A.; Herwig, P.; Müllen, K.; Rabe, J. P. Diodelike current—voltage curves for a single molecule—tunneling spectroscopy with submolecular resolution of an alkylated, *peri*-condensed hexabenzocoronene. *Angew. Chem., Int. Ed.* **1995**, 34 (15), 1609—1611
- (32) Watson, M. D.; Fechtenkötter, A.; Müllen, K. Big is beautiful—"aromaticity" revisited from the viewpoint of macromolecular and supramolecular benzene chemistry. *Chem. Rev.* **2001**, *101* (5), 1267–1300.
- (33) Ito, H.; Segawa, Y.; Murakami, K.; Itami, K. Polycyclic arene synthesis by annulative  $\pi$ -extension. *J. Am. Chem. Soc.* **2019**, *141* (1), 3–10.
- (34) Borissov, A.; Maurya, Y. K.; Moshniaha, L.; Wong, W.-S.; Żyła-Karwowska, M.; Stępień, M. Recent advances in heterocyclic nanographenes and other polycyclic heteroaromatic compounds. *Chem. Rev.* **2022**, *122* (1), 565–788.
- (35) Englert, J. M.; Malig, J.; Zamolo, V. A.; Hirsch, A.; Jux, N. HBC-porphyrin close contact chromophores. *Chem. Commun.* **2013**, 49 (42), 4827–4829.
- (36) Lungerich, D.; Hitzenberger, J. F.; Marcia, M.; Hampel, F.; Drewello, T.; Jux, N. Superbenzene-porphyrin conjugates. *Angew. Chem., Int. Ed.* **2014**, 53 (45), 12231–12235.
- (37) Martin, M. M.; Lungerich, D.; Haines, P.; Hampel, F.; Jux, N. Electronic communication across porphyrin hexabenzocoronene isomers. *Angew. Chem., Int. Ed.* **2019**, *58* (26), 8932–8937.
- (38) Martin, M. M.; Lungerich, D.; Hampel, F.; Langer, J.; Ronson, T. K.; Jux, N. Multiple-porphyrin functionalized hexabenzocoronenes. *Chem. Eur. J.* **2019**, *25* (66), 15083–15090.
- (39) Ruppel, M.; Gazetas, L.-P.; Lungerich, D.; Jux, N. Synthesis and photophysical properties of hexabenzocoronene-tetrabenzoporphyrin architectures. *Eur. J. Org. Chem.* **2020**, 2020 (40), 6352–6360.
- (40) Wolf, M.; Lungerich, D.; Bauroth, S.; Popp, M.; Platzer, B.; Clark, T.; Anderson, H. L.; Jux, N.; Guldi, D. M. Panchromatic light funneling through the synergy in hexabenzocoronene—(metallo)-porphyrin—fullerene assemblies to realize the separation of charges. *Chem. Sci.* **2020**, *11* (27), 7123–7132.
- (41) Haines, P.; Kaur, R.; Martin, M. M.; Minameyer, M. B.; Frühwald, S.; Bönisch, S.; Lungerich, D.; Hampel, F.; Görling, A.; Drewello, T.; Jux, N.; Guldi, D. M. Screening nanographene-mediated inter(porphyrin) communication to optimize inter(porphyrin–fullerene) forces. *Adv. Energy Mater.* 2021, *11* (17), No. 2100158.
- (42) Hölzel, H.; Haines, P.; Kaur, R.; Lungerich, D.; Jux, N.; Guldi, D. M. Probing charge management across the π-systems of

- nanographenes in regioisomeric electron donor-acceptor architectures. J. Am. Chem. Soc. 2022, 144 (20), 8977-8986.
- (43) Wong, W. W. H.; Khoury, T.; Vak, D.; Yan, C.; Jones, D. J.; Crossley, M. J.; Holmes, A. B. A porphyrin-hexa-*peri*-hexabenzocoronene-porphyrin triad: Synthesis, photophysical properties and performance in a photovoltaic device. *J. Mater. Chem.* **2010**, *20* (33), 7005–7014.
- (44) Chen, Q.; Brambilla, L.; Daukiya, L.; Mali, K. S.; De Feyter, S.; Tommasini, M.; Müllen, K.; Narita, A. Synthesis of triply fused porphyrin-nanographene conjugates. *Angew. Chem., Int. Ed.* **2018**, *57* (35), 11233–11237.
- (45) Umeyama, T.; Hanaoka, T.; Yamada, H.; Namura, Y.; Mizuno, S.; Ohara, T.; Baek, J.; Park, J.; Takano, Y.; Stranius, K.; Tkachenko, N. V.; Imahori, H. Exclusive occurrence of photoinduced energy transfer and switching of its direction by rectangular  $\pi$ -extension of nanographenes. *Chem. Sci.* **2019**, 10 (27), 6642–6650.
- (46) Wang, Z.; Dötz, F.; Enkelmann, V.; Müllen, K. Double-concave" graphene: Permethoxylated Hexa-peri-hexabenzocoronene and its cocrystals with hexafluorobenzene and fullerene. *Angew. Chem., Int. Ed.* **2005**, 44 (8), 1247–1250.
- (47) Tremblay, N. J.; Gorodetsky, A. A.; Cox, M. P.; Schiros, T.; Kim, B.; Steiner, R.; Bullard, Z.; Sattler, A.; So, W. Y.; Itoh, Y.; Toney, M. F.; Ogasawara, H.; Ramirez, A. P.; Kymissis, I.; Steigerwald, M. L.; Nuckolls, C. Photovoltaic universal joints: Ball-and-socket interfaces in molecular photovoltaic cells. *ChemPhysChem* **2010**, *11* (4), 799–803.
- (48) Chiu, C.-Y.; Kim, B.; Gorodetsky, A. A.; Sattler, W.; Wei, S.; Sattler, A.; Steigerwald, M.; Nuckolls, C. Shape-shifting in contorted dibenzotetrathienocoronenes. *Chem. Sci.* **2011**, *2* (8), 1480–1486.
- (49) Yang, Y.; Cheng, K.; Lu, Y.; Ma, D.; Shi, D.; Sun, Y.; Yang, M.; Li, J.; Wei, J. A polyaromatic nano-nest for hosting fullerenes  $C_{60}$  and  $C_{70}$ . Org. Lett. **2018**, 20 (8), 2138–2142.
- (50) Lu, D.; Zhuang, G.; Wu, H.; Wang, S.; Yang, S.; Du, P. A large  $\pi$ -extended carbon nanoring based on nanographene units: Bottom-up synthesis, photophysical properties, and selective complexation with fullerene  $C_{70}$ . Angew. Chem., Int. Ed. 2017, 56 (1), 158–162.
- (51) Huang, Q.; Zhuang, G.; Jia, H.; Qian, M.; Cui, S.; Yang, S.; Du, P. Photoconductive curved-nanographene/fullerene supramolecular heterojunctions. *Angew. Chem., Int. Ed.* **2019**, *58* (19), *6244*–*6249*.
- (52) Zank, S.; Fernandez-Garcia, J. M.; Stasyuk, A. J.; Voityuk, A. A.; Krug, M.; Sola, M.; Guldi, D. M.; Martín, N. Initiating electron transfer in doubly curved nanographene upon supramolecular complexation of  $C_{60}$ . Angew. Chem., Int. Ed. 2022, 61 (7), No. e202112834.
- (53) Jiménez, V. G.; David, A. H. G.; Cuerva, J. M.; Blanco, V.; Campana, A. G. A macrocycle based on a heptagon-containing Hexaperi-hexabenzocoronene. *Angew. Chem., Int. Ed.* **2020**, *59* (35), 15124–15128.
- (54) Chang, X.; Xu, Y.; von Delius, M. Recent advances in supramolecular fullerene chemistry. *Chem. Soc. Rev.* **2024**, DOI: 10.1039/D2CS00937D.
- (55) Sygula, A.; Fronczek, F. R.; Sygula, R.; Rabideau, P. W.; Olmstead, M. M. A double concave hydrocarbon buckycatcher. *J. Am. Chem. Soc.* **2007**, *129* (13), 3842–3843.
- (56) Takeda, M.; Hiroto, S.; Yokoi, H.; Lee, S.; Kim, D.; Shinokubo, H. Azabuckybowl-based molecular tweezers as  $C_{60}$  and  $C_{70}$  receptors. *J. Am. Chem. Soc.* **2018**, *140* (20), 6336–6342.
- (57) Sacristán-Martín, A.; Barbero, H.; Ferrero, S.; Miguel, D.; Garcia-Rodriguez, R.; Alvarez, C. M. On/off metal-triggered molecular tweezers for fullerene recognition. *Chem. Commun.* **2021**, 57 (84), 11013–11016.
- (58) Cha, W.-Y.; Ahn, A.; Kim, T.; Oh, J.; Ali, R.; Park, J. S.; Kim, D. Changes in macrocyclic aromaticity and formation of a charge-separated state by complexation of expanded porphyrin and  $C_{60}$ . Chem. Commun. **2019**, 55 (57), 8301–8304.